Carrier-Envelope-Phase Controlled Attosecond Pulse Generation by Undulator Radiation

Zoltán Tibai[1]*, György Tóth[1], Anett Nagyváradi[2], András Gyöngy[1], József András Fülöp[3,4], János Hebling[1,3,4] and Gábor Almási[1,3]

[1] Institute of Physics, University of Pécs, Pécs, Hungary, [2] Faculty of Engineering and Information Technology, University of Pécs, Pécs, Hungary, [3] MTA-PTE High-Field Terahertz Research Group, Pécs, Hungary, [4] Szentágothai Research Centre, University of Pécs, Pécs, Hungary

Practical aspects of the robust method we proposed for producing few-cycle attosecond pulses with arbitrary waveform in the extreme ultraviolet spectral range are studied numerically. It is based on the undulator radiation of relativistic ultrathin electron layers produced by laser-driven energy modulation. By using realistic specifications, we show that isolated waveform-controlled extreme ultraviolet attosecond pulses at 5 nm with 10 nJ energy and 20 as pulse duration, at 20 nm with 90 nJ energy and 80 as pulse duration, and at 60 nm with 200 nJ energy and 240 as duration can be generated, respectively.

PACS numbers: 41.60.Cr, 41.50.+h, 41.75.Ht

Keywords: free elecron lasers, attosecond, carrier-envelope-phase, waveform, undulator radiation

INTRODUCTION

In recent years a few phenomena sensitive to the carrier-envelope-phase (CEP) of ultrashort laser pulses were recognized [1, 2]. Waveform-controlled few-cycle laser pulses enabled the generation of isolated attosecond pulses in the extreme ultraviolet (EUV) spectral range and their application to the study of electron dynamics in atoms, molecules, and solids [3]. The observation of inner-atomic (strong-field) phenomena and EUV pump—EUV probe measurements require intense CEP-controlled attosecond pulses [4–6]. EUV pump—EUV probe experiments can be carried out at free-electron lasers (FELs) [7, 8]; however, the temporal resolution is limited to the few fs regime.

Various schemes, such as the longitudinal space charge amplifier [9], emittance spoiler foil technique [10, 11], wave selection technique [12], or enhanced self-amplified spontaneous emission (E-SASE) [13, 14], were proposed for attosecond pulse generation at FELs. High current modulation technique were suggested to generate isolated attosecond pulses in X-ray region [15, 16]. Recently described schemes suggest the possibility of sub-attosecond pulse generation in the hard-X-ray region [17], and single-cycle FEL pulse generation in the THz [18] and in the X-ray region [19].

However, the stochastic pulse shape predicted for the pulses generated by these methods is disadvantageous. Furthermore, there are no reliable techniques available for CEP control of these or any other attosecond pulse sources. In contrast, recently we proposed and numerically investigated a robust method for producing waveform-controlled linearly and circularly polarized CEP-stable attosecond pulses in the EUV spectral range [20–22]. The analytical investigation of this concept was carried out by Shamuilov et al. [23]. It uses relativistic electron bunches from a

linear accelerator (LINAC), and relies on ultrathin nanoscale-length electron layers (nanobunches) generated by laser-driven energy modulation, and on undulator radiation. In this setup waveform-controlled attosecond pulse generation is possible, unparalleled by other similar setups, where the predicted pulse energy and the short wavelength are imposing, but the waveform is stochastic [14].

In the present paper, a more detailed investigation is carried out on the feasibility of this technique. Practically important aspects were numerically studied. The dependence of the attosecond pulse energy on the radiation wavelength, and undulator parameter were also studied, together with a possible way for isolated attosecond pulse generation.

THE INVESTIGATED SETUP AND THE SIMULATION METHODS

The scheme of the setup proposed in Ref. [20] and further investigated in this work is shown in **Figure 1**. This scheme is very similar to the ultrahigh harmonics generation scheme of Ref. [24], which is the simplest version of the high gain harmonic generation (HGHG) technique, however, there is no gain in the modulator. Recently such a scheme was further investigated [25], and it was shown that according to the calculation generation of harmonics to an order as high as 1000 is possible. In order to generate coherent attosecond pulses, nanometer scale electron modulation is needed. Thus, the FEL community investigated and proposed some sophisticated modulation techniques, such as the π shifter technique [26], echo-enabled harmonic generation (EEHG) [27] or cooled HGHG [28], which increase the frequency up-conversion efficiency.

In our scheme the simplest combination, i.e., one modulator (MU) and one radiator (RU) undulator were used. Compared to Ref. [24, 25], our scheme uses a radiator undulator that consists only of a few periods (no exponential gain inside), and the generated radiation wavelength is arbitrary, i.e., independent from the wavelength of the modulator laser (which is usually called the seed). Furthermore, in our calculations we investigated the temporal shape of the radiation field (not only its spectrum).

In our modell the relativistic electron beam from a LINAC is sent through a modulator undulator where a TW-power laser beam is superimposed on it and introduces a periodic energy modulation of the electrons along the longitudinal (z) direction. This energy modulation leads to the formation of nanobunches at the end of the chicane behind the MU. Evidently, efficient generation of coherent and non-stochastic radiation pulses is possible only if the nanobunch length is shorter than the half period of the radiation. As our aim was to generate coherent EUV radiation in the 10 to 100 nm wavelength range, the minimization of the nanobunch length down to the sub-10-nm range was essential.

The nanobunched electron beam then passes through the radiator undulator consisting of a single period or of a few periods, depending on the desired waveform, and it emits electromagnetic radiation. The entrance of the RU is placed behind the MU at a position where the nanobunch length is the

shortest. The wavelength of the generated radiation is determined by the well-known resonance condition [29]

$$\lambda_r = \frac{\lambda_{RU} \cdot \left(1 + \frac{K_{RU}^2}{2}\right)}{2\gamma^2}. \tag{1}$$

Here, λ_r is the wavelength of the generated EUV radiation, λ_{RU} is the period of the RU, $K_{RU} = \frac{eB_{0,RU}\lambda_{RU}}{2\pi mc}$ is the undulator parameter, $B_{0,RU}$ is the peak magnetic field of the RU, e and m are the electron charge and mass, respectively, γ is the relativistic factor, and c is the speed of light. The generated radiation waveform is mainly determined by the magnetic field distribution of the RU along the electron beam propagation direction z. For a better comparison of the EUV pulse parameters obtained in the different cases investigated below, the same RU magnetic field distribution

$$B_{RU} = \begin{cases} B_{0,RU} \, e^{-\frac{z^2}{2w_{RU}^2}} \cos\left(\frac{2\pi}{\lambda_{RU}}z\right), & \text{if } -\frac{L}{2} < z < \frac{L}{2}, \\ 0, & \text{otherwise} \end{cases} \tag{2}$$

was used throughout this work (see also **Figure 1**). Here, w_{RU} is the width of the Gaussian envelope and L is the length of the RU. These parameters were set to $w_{RU} = 1.5 \cdot \lambda_{RU}$ and $L = 2.5 \cdot \lambda_{RU}$.

In order to consider a realistic situation, the initial electron bunches (**Table 1**) were used according to the start to end (S2E) simulation of the accelerator of FLASH at DESY in Germany [30–34]. In the energy modulation we assumed a double-period MU with TW-level modulator laser, where ELEGANT [35] and CSRTrack [36] codes were used for the numerical simulation. In the radiator undulator, a similar theoretical model and simulation tools were used as in Ref. [20]. In our calculations we investigated 100 pC and 1000 pC charge scenarios of the FLASH accelerator, where 200,000 and one million macroparticles per bunch were used, respectively (see **Table 1**).

When the Coulomb interaction is neglected an approximate expression for the full width at half-maximum (FWHM) length of the nanobunch, Δz_0, can be given by analytical derivation [14, 37]:

$$\Delta z_0 \approx \frac{1}{2}\frac{\lambda_L}{A}. \tag{3}$$

The relative energy modulation is given by $A = \Delta\gamma/\sigma_\gamma$, where $\sigma_\gamma = \sigma_\gamma^* \gamma$ is the intrinsic energy spread (**Table 1**) and $\Delta\gamma$ is the energy modulation acquired in the MU owing to energy modulation. At large relative modulation ($A \gg 1$) the nanobunch becomes much shorter than the laser wavelength.

TW-class table-top light sources with pulse durations comprising only a few optical cycles were intensely developed during the last few years [38, 39]. For example, Herrmann et al. [38] reported a two-stage non-collinear optical parametric chirped-pulse amplification (OPCPA) system generating 16-TW, sub-three-cycle (130-mJ, 7.9-fs) pulses at an 805 nm central wavelength. Suitable light pulse sources are also being constructed elsewhere, for example in the Extreme Light Infrastructure (ELI) project [39]. Here we note that for $\lambda_r \gtrsim 20$ nm EUV wavelengths $\lambda_L \approx 800$ nm gives higher
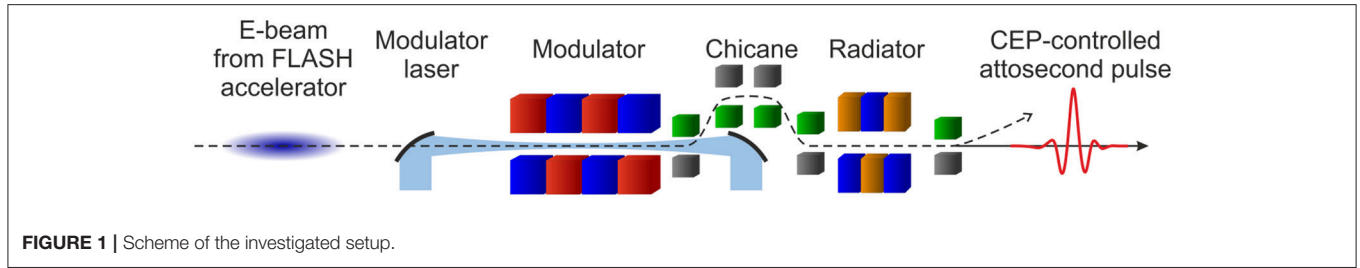
FIGURE 1 | Scheme of the investigated setup.

TABLE 1 | Parameters used in the simulations with 100 pC and 1000 pC bunch charges.

Parameter	Value	Value
E-beam energy (γ)	1,955	1,955
E-beam relative slice energy spread ($\sigma_\gamma {}^*$)	0.03 %	0.015 %
Bunch charge	100 pC	1000 pC
Peak current	2.1 kA	2.5 kA
E-beam length	30 μm	160 μm
E-beam normalized slice emittance	0.45 mm mrad	1.1 mm mrad
E-beam radius	80 μm	80 μm
Laser wavelength (λ_L)	516 nm	516 nm
Laser peak power	10 TW	10 TW
Laser beam waist inside MU	0.5 mm	0.5 mm

EUV pulse energies. Only below ∼20 nm is the choice of a shorter laser wavelength (i.e., 516 nm, **Table 1**) advantageous, because of the shorter nanobunches. Though TW-class few-cycle OPCPA systems around 500 nm central wavelength need yet to be demonstrated, promising techniques are being developed [40–42]. In section III.B we consider the possibilities for isolated attosecond EUV pulse generation, where laser pulses as short as two optical cycles are needed. For the generation of attosecond pulse trains longer laser pulses can be used.

We used the following handbook formula to calculate the electric field of the radiation generated in the RU [43]:

$$\overrightarrow{E}\left(t, \overrightarrow{r}\right) = \sum \left[\frac{q\mu_0}{4\pi} \frac{\overrightarrow{R} \times \left(\left(\overrightarrow{R} - R\overrightarrow{\beta}\right) \times \dot{\overrightarrow{v}}\right)}{\left(R - \overrightarrow{R} \cdot \overrightarrow{\beta}\right)^3} \right]_{ret}, \quad (4)$$

where μ_0 is the vacuum permeability, q is the macroparticle charge, $\overrightarrow{R}$ is the vector pointing from the position of the macroparticle at the retarded moment to the observation point, $\overrightarrow{v}$ is the velocity of the macroparticle, $\overrightarrow{\beta} = \frac{\overrightarrow{v}}{c}$, c is the speed of light. The summation is for all macroparticles. During the radiation process the position, velocity, and acceleration of the macroparticles were traced numerically by taking into account the Lorentz force of the magnetic field of RU. The Coulomb interaction between the macroparticles was neglected during the undulator radiation process, because the transversal electron motion is by four orders of magnitude larger than the motion generated by Coulomb interaction.

RESULTS

Nanobunch Generation

The energy modulation with a high power laser in the MU and the chicane was calculated with ELEGANT and CSRTrack codes, respectively. Despite the use of a TW-level modulator laser, in our calculation a chicane was also used, because it can control the position of the spatial focus of the nanobunch and allows to feed out the modulator laser pulses. The result of the nanobunches in case of 11 different simulations (gray) and their average (red) are shown in **Figure 2** after the chicane for $P_L = 10$ TW laser power, in 100 pC and 1000 pC cases, respectively. The obtained energy modulation was $\Delta_\gamma = 134$ at $K_{MU} = 1.4$ and $\lambda_{MU} = 1.99$ m. The charge of a single nanobunches are 1.1 pC and 1.0 pC and their lengths are as short as 6 nm and 4 nm at 1.25 m behind the end of the modulator undulator. These nanobunches were used in the further calculations to obtain the EUV pulses described in section III.B.

EUV Pulse Generation

The temporal shape of the attosecond EUV pulses emitted by the extremely short electron nanobunches in the RU were calculated at a plane positioned 8 m behind the RU center. The EUV waveform can be conveniently set by the magnetic field distribution of the RU [20]. The distribution of the magnetic field of the RU (blue) and the average of the electric field of the attosecond pulses (red) are shown in **Figure 3** for 100 pC and 1000 pC cases, respectively.

The emphasis was on exploring the dependence of the EUV pulse energy on important experimental parameters such as radiation wavelength and RU undulator parameter. The EUV pulse energy as function of the radiation wavelength (λ_r) in the range of 20 ÷ 200 nm is shown in **Figure 4**, and two different RU undulator parameter values (0.5 and 0.8). The larger EUV pulse energy is obtained with the larger K_{RU}. The undulator parameter can be set to the desired value by adjusting the magnetic field amplitude. The radiation wavelength, given by the resonance condition Equation (1), can be set by the choice of the RU period λ_{RU}. As seen in **Figure 4**, the pulse energy first increases with increasing wavelength, followed by saturation and subsequent energy decrease. The reason of the latter is the longer undulator period needed to generate longer wavelengths. Due to the associated longer path inside the RU the average nanobunch length and transversal size increases [21], thereby reducing
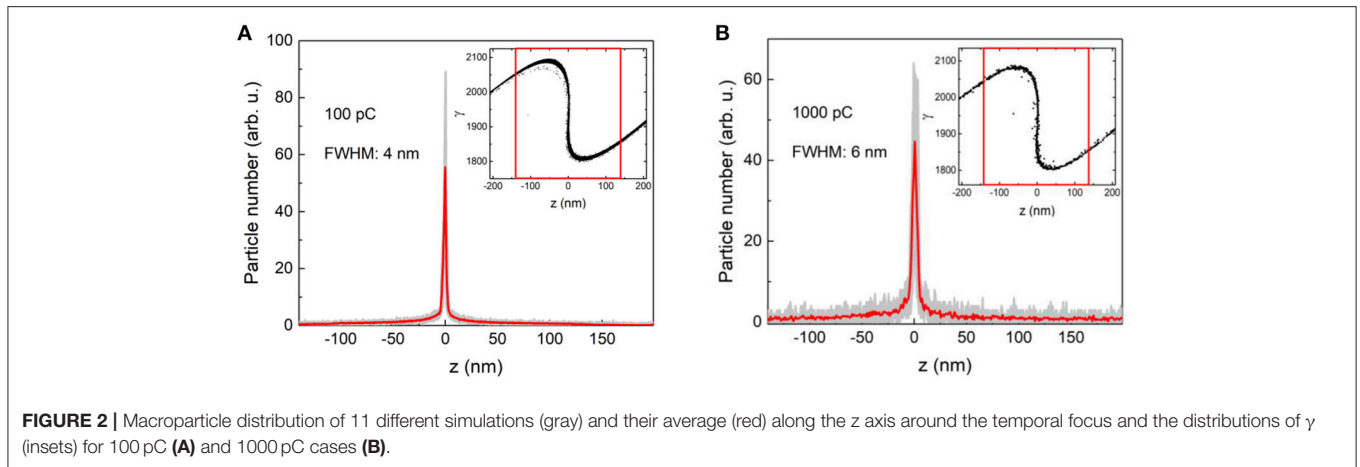
FIGURE 2 | Macroparticle distribution of 11 different simulations (gray) and their average (red) along the z axis around the temporal focus and the distributions of γ (insets) for 100 pC **(A)** and 1000 pC cases **(B)**.
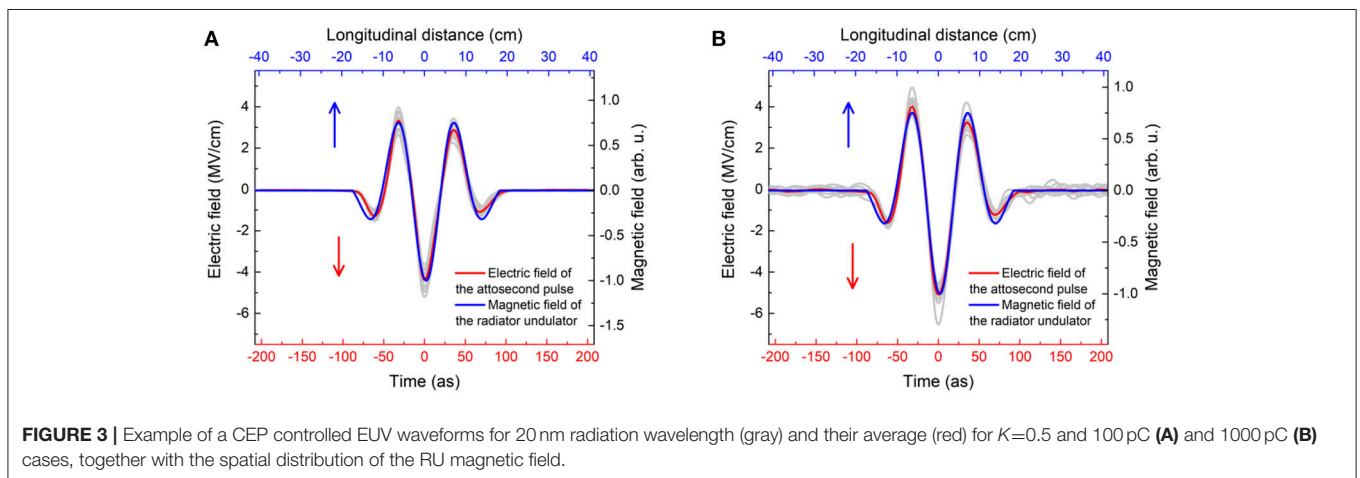

FIGURE 3 | Example of a CEP controlled EUV waveforms for 20 nm radiation wavelength (gray) and their average (red) for $K = 0.5$ and 100 pC **(A)** and 1000 pC **(B)** cases, together with the spatial distribution of the RU magnetic field.
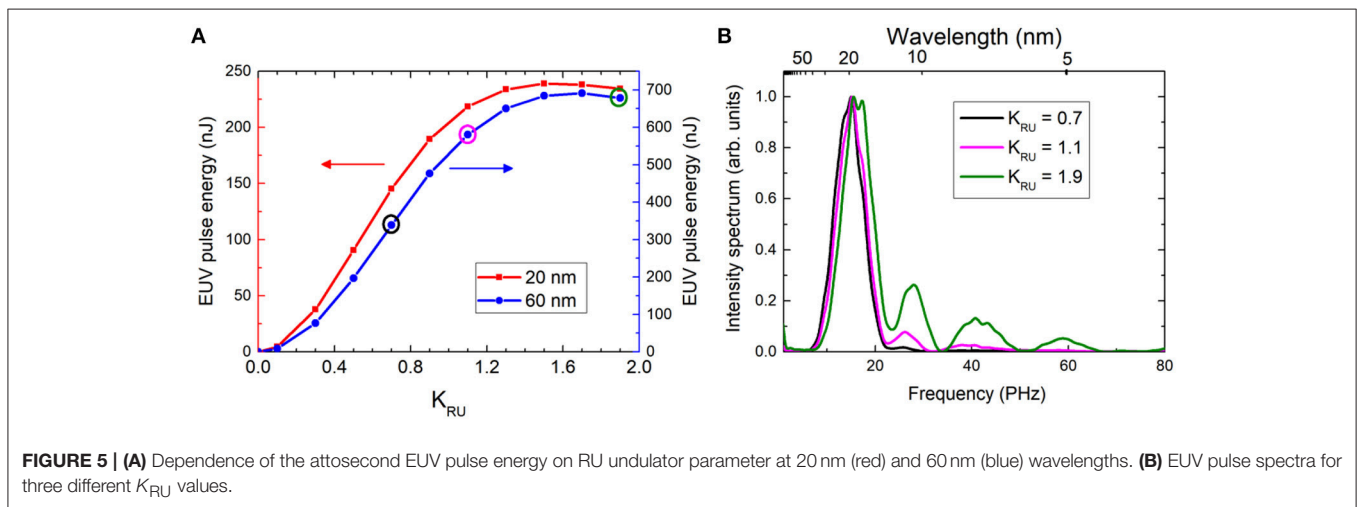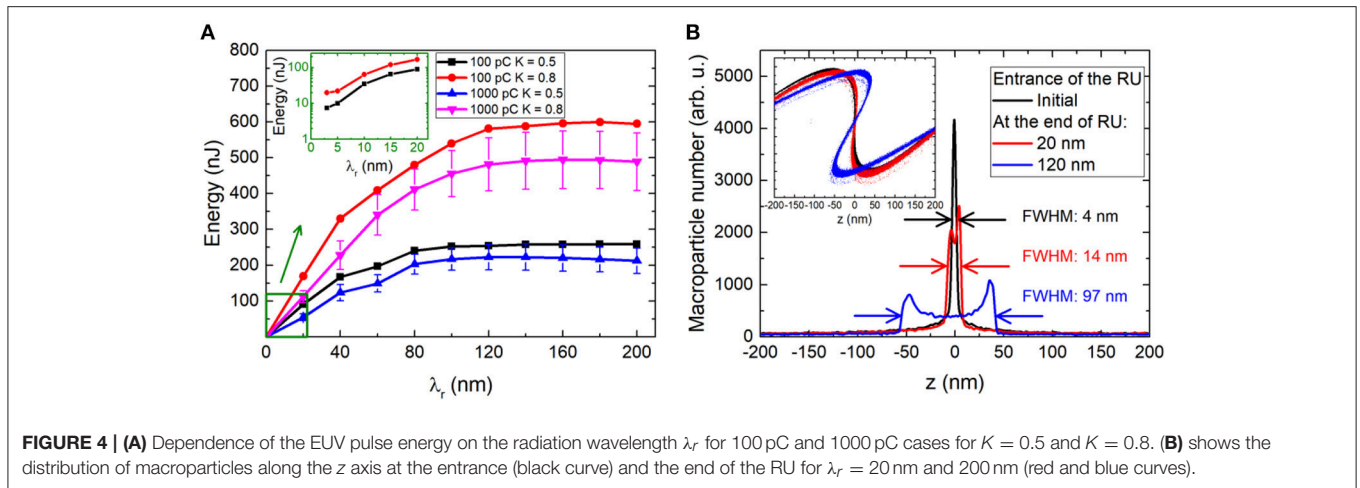
coherence in the radiation process. As shown in **Figure 4B** for 20 and 120 nm cases, the nanobunch lengths are increased by 350 and 2,400% at the end of the radiator undulator (red and blue curves), respectively. We note that for the generation of waveform-controlled pulses at longer wavelengths longer nanobunches (and lower modulator laser power) can be used more advantageously.

In the second calculation series the electron bunch with 100 pC was used and the RU undulator parameter was varied in the range of $K_{RU} = 0.1 \div 1.9$ and the λ_{RU} undulator period was chosen such that for each value of K_{RU} the radiation wavelength was kept at 20 and 60 nm, respectively. For both wavelengths, the EUV pulse energy is proportional to K_{RU}^2 below about $K_{RU} = 0.7$, followed by saturation at larger K_{RU} (**Figure 5A**). The reason of the saturation is that a larger K_{RU} results in more pronounced harmonics of the radiation wavelength (see **Figure 5B**, where the spectra of the EUV pulses for three different K_{RU} values for the 20-nm case is shown). However, the spectral components of the shorter wavelengths are suppressed by the destructive interference, which results in the saturation of the energy.

According to the calculations, single-cycle 20-as pulses with more than 10 nJ energy at 5 nm, 80-as pulses with more than

200 nJ energy at 20 nm, and 240-as pulses with more than 650 nJ energy at 60 nm can be generated.

Since in our setup the electron bunch consists of multiple nanobunches separated by the modulation laser wavelength, a pulse sequence is generated. The ratio of separation time to pulse duration is smaller than 40. This can be too small for certain applications. One possibility for increasing this ratio substantially is to use two modulation lasers with significantly different wavelengths [13, 44]. We investigated another possibility for isolated CEP stable attosecond pulse generation, namely the shortening of the modulator pulse duration. The modulator laser produces an energy modulation with a temporal profile that closely resembles the waveform of the laser electric field. We assumed a sine-like waveform, corresponding to zero CEP and zero energy modulation at the maximum of the laser pulse envelope, like in Ref. [13, 14]. The energy modulation produces current modulations, where a central and an even number of satellite peaks occure (the corresponding satellite peak amplitudes are substantially similar). In our simulations, the modulator laser pulses consist only of a few optical cycles (**Figure 6A**). **Figure 6B** shows the calculated waveform of the main attosecond pulse and the neighboring satellite pulses

FIGURE 4 | (A) Dependence of the EUV pulse energy on the radiation wavelength λ_r for 100 pC and 1000 pC cases for $K = 0.5$ and $K = 0.8$. **(B)** shows the distribution of macroparticles along the z axis at the entrance (black curve) and the end of the RU for $\lambda_r = 20$ nm and 200 nm (red and blue curves).

FIGURE 5 | (A) Dependence of the attosecond EUV pulse energy on RU undulator parameter at 20 nm (red) and 60 nm (blue) wavelengths. **(B)** EUV pulse spectra for three different K_{RU} values.

for a few different modulator laser pulse durations. As the modulating pulse duration is decreased below about 5 cycles or 8 fs the peak amplitude of the satellite attosecond pulses start to significantly decrease. Modulator pulses with less than about 2.0 cycles or 3.4 fs are able to generate CEP stable isolated attosecond pulses. In this case, the energy of the satellite pulses is only about 1–2% of the main attosecond pulse. We have to note that the CEP of the modulator pulse strongly influences the degree of isolation of the generated attosecond pulse. However, it does not determine the CEP of the attosecond pulse.

Finally, we compare our results to the experimental performance of attosecond EUV pulse sources based on high-order harmonic generation (HHG) in gas or plasma driven by high-intensity optical pulses [3, 45]. Isolated attosecond pulses (IAPs) can be generated by few-cycle driving pulses or by using gating techniques with longer pulses [45]. Typical IAP energies are in the sub-nJ to 10 nJ range. The shortest pulse duration reported to date was 67 as; the wavelength range was ∼10 to 20 nm [46]. CEP-stable single-cycle 130-as

IAPs were reported with an estimated CEP fluctuation of 140 mrad [43]. However, no pulse energy was given in these works [45–47]. Recently, the generation of 500-as IAPs with 1.3 μJ energy at ∼30 eV was demonstrated [48]. Trains of attosecond pulses with an energy on the μJ scale can be generated by using many-cycle driving pulses. Significantly higher pulse and photon energies are expected from laser-produced plasmas [45, 49], though the full potential of this method needs yet to be demonstrated.

In comparison, as shown above, similar shortest pulse durations can be achieved with our method as by HHG, at comparable wavelengths. However, unparalleled by any other source reported so far, our method easily enables the full control of the attosecond pulse waveform.

CONCLUSION

In summary, practical aspects of the method proposed in our previous work [20] for stable arbitrary-waveform attosecond
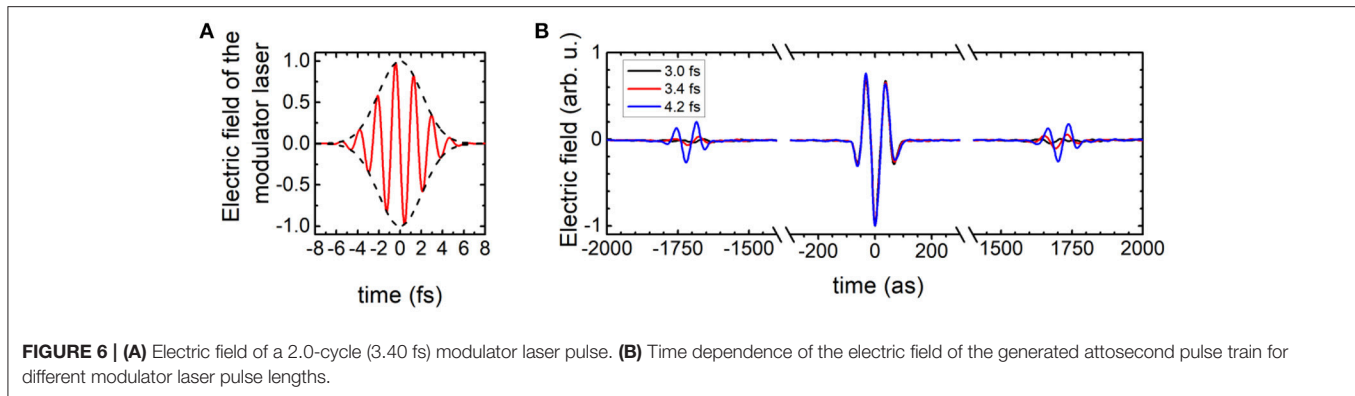
FIGURE 6 | (A) Electric field of a 2.0-cycle (3.40 fs) modulator laser pulse. **(B)** Time dependence of the electric field of the generated attosecond pulse train for different modulator laser pulse lengths.

EUV pulse generation were investigated in detail by means of numerical simulations. The scaling of the generated attosecond EUV pulse energy with various parameters (λ_r, K_{RU}) was studied. For example, the nanobunches were predicted to emit 20-as EUV pulses at $\lambda_r = 5$ nm with 10 nJ energy, 80-as EUV pulses at $\lambda_r = 20$ nm with 90 nJ energy, and 240-as pulses at $\lambda_r = 60$ nm with 200 nJ energy for $K_{RU} = 0.5$. At longer generated wavelength or larger K_{RU} the generation of EUV pulses with more than 500 nJ energy can be possible. The shortening of the modulator laser pulse duration was discussed for the generation of isolated attosecond pulses.

The proposed scheme can enable the development of practical sources of CEP stable attosecond EUV pulses using existing LINACs. These unprecedented pulses can be used for example in EUV pump—EUV probe experiments in the near future.

REFERENCES

1. Dombi P, Krausz F, Farkas G. Ultrafast dynamics and carrier-envelope phase sensitivity of multiphoton photoemission from metal surfaces. *J Mod Opt.* (2006) **53:**163–72. doi: 10.1080/09500340500159708

2. Wittmann T, Horvath B, Helml W, Schätzel MG, Gu X, Cavalieri AL, et al. R. Single-shot carrier–envelope phase measurement of few-cycle laser pulses. *Nat Phys.* (2009) **5:**357–62. doi: 10.1038/nphys1250

3. Krausz F, Ivanov M. Attosecond physics. *Rev Mod Phys.* (2009) **81:**163. doi: 10.1103/RevModPhys.81.163

4. Peng LY, Starace AF. Attosecond pulse carrier-envelope phase effects on ionized electron momentum and energy distributions. *Phys Rev A* (2007) **76:**043401. doi: 10.1103/PhysRevA.76.043401

5. Liu C, Reduzzi M, Trabattoni A, Sunilkumar A, Dubrouil A, Calegari F, et al. Carrier-envelope phase effects of a single attosecond pulse in two-color photoionization. *Phys Rev Lett.* (2013) **111:**123901. doi: 10.1103/PhysRevLett.111.123901

6. Borbély S, Tóth A, Tőkési K, Nagy L. Spatial and temporal interference during the ionization of H by few-cycle XUV laser pulses. *Phys Rev A* (2013) **87:**013405. doi: 10.1103/PhysRevA.87.013405

7. Jiang YH, Rudenko A, Herrwerth O, Foucar L, Kurka M, Kühnel KU, et al. Ultrafast extreme ultraviolet induced isomerization of acetylene cations. *Phys. Rev. Lett.* (2010) **105:**263002. doi: 10.1103/PhysRevLett.105.263002

8. Magrakvelidze M, Herrwerth O, Jiang YH, Rudenko A, Kurka M, Foucar L, et al. Tracing nuclear-wave-packet dynamics in singly and doubly charged states of N_2 and O_2 with XUV-pump–XUV-probe experiments. *Phys Rev A* (2012) **86:**013415. doi: 10.1103/PhysRevA.86.013415

9. Marinelli A, Hemsing E, Rosenzweig JB. Using the relativistic two-stream instability for the generation of soft-x-ray attosecond radiation pulses. *Phys Rev Lett.* (2013) **110:**064804. doi: 10.1103/PhysRevLett.110.064804

10. Marinellia MacArthur J, Emma P, Guetg M, Field C, Kharakh D, Lutman AA, et al. Experimental demonstration of a single-spike hard-X-ray free-electron laser starting from noise. *Appl Phys Lett.* (2017) **111:**151101. doi: 10.1063/1.4990716

11. Emma P, Bane K, Cornacchia M, Huang Z, Schlarb H, Stupakov G, et al. Femtosecond and subfemtosecond X-ray pulses from a self-amplified spontaneous-emission–based free-electron laser. *Phys Rev Lett.* (2004) **92:**074801. doi: 10.1103/PhysRevLett.92.074801

12. Saldin EL, Schneidmiller EA, Yurkov MV. Terawatt-scale sub-10-fs laser technology–key to generation of GW-level attosecond pulses in X-ray free electron laser. *Opt Commun.* (2004) **237:**153–164. doi: 10.1016/j.optcom.2004.03.070

13. Zholents AA, Penn G. Obtaining attosecond x-ray pulses using a self-amplified spontaneous emission free electron laser. *Phys Rev.* (2005) **8:**050704. doi: 10.1103/PhysRevSTAB.8.050704

14. Zholents Z. Method of an enhanced self-amplified spontaneous emission for x-ray free electron lasers. *Phys Rev.* (2005) **8:**040701. doi: 10.1103/PhysRevSTAB.8.040701

15. Kumar S, Parc YW, Landsman AS, Kim DE. Temporally-coherent terawatt attosecond XFEL synchronized with a few cycle laser. *Sci Rep.* (2016) **6:**37700. doi: 10.1038/srep37700

16. Shim CH, Parc YW, Kumar S, Ko I, S, Kim DE. Isolated terawatt attosecond hard X-ray pulse generated from single current spike. *Sci Rep.* (2018) **8:**7463. doi: 10.1038/s41598-018-25778-x

17. Dunning DJ, McNeil B, WJ, Thompson NR. Coherence and Raman sideband cooling of a single atom in an optical tweezer. *Phys Rev Lett.* (2013) **110**:104801. doi: 10.1103/PhysRevLett.110.104801

18. Goryashko VA. Quasi-half-cycle pulses of light from a tapered undulator. *Phy Rev.* (2017) **20**:080703. doi: 10.1088/1742-6596/488/3/032022

19. Tanaka T. Proposal to generate an isolated monocycle x-ray pulse by counteracting the slippage effect in free-electron lasers. *Phys Rev Lett.* (2015) **114**:044801. doi: 10.1103/PhysRevLett.114.044801

20. Tibai Z, G Tóth, Mechler MI, Fülöp JA, Almási G, Hebling J. Proposal for carrier-envelope-phase stable single-cycle attosecond pulse generation in the extreme-ultraviolet range. *Phys Rev Lett.* (2014) **113**:104801. doi: 10.1103/PhysRevLett.113.104801

21. Tóth G, Tibai Z, Nagy-Csiha Z, Márton Z, Almási G, Hebling J. Circularly polarized carrier-envelope-phase stable attosecond pulse generation based on coherent undulator radiation. *Opt Lett.* (2015) **40**:4317–20. doi: 10.1364/OL.40.004317

22. Tibai Z, Tóth G, Nagy-Csiha Z, Fülöp JA, Almási G, Hebling J, et al. Investigation of the newly proposed carrier-envelope-phase stable attosecond pulse source. *arXiv:1604.08050* (2016).

23. Shamuilov G, Mak A, Salén P, Goryashko V. Analytical model of waveform-controlled single-cycle light pulses from an undulator. *Opt Lett.* (2018) **43**:819–22. doi: 10.1364/OL.43.000819

24. Goloviznin VV, van Amersfoort PW. Generation of ultrahigh harmonics with a two-stage free electron laser and a seed laser. *Phys Rev E* (1997) **55**:6002. doi: 10.1103/PhysRevE.55.6002

25. Deng HX, Dai ZM. Ultra-high order harmonic generation via a free electron laser mechanism. *Chinese Phys C* (2010). **34**:1140. doi: 10.1088/1674-1137/34/8/020

26. Allaria E, De Ninno G. Soft-X-ray coherent radiation using a single-cascade free-electron laser. *Phys Rev Lett.* (2007) **99**:014801. doi: 10.1103/PhysRevLett.99.014801

27. Xiang D, Stupakov G. Echo-enabled harmonic generation free electron laser. *Phys Rev.* (2009) **12**:030702. doi: 10.1103/PhysRevSTAB.12.030702

28. Deng HX, Feng C. Using off-resonance laser modulation for beam-energy-spread cooling in generation of short-wavelength radiation. *Phys Rev Lett.* (2013) **111**:084801. doi: 10.1103/PhysRevLett.111.084801

29. Schmüser P, Dohlus M, Rossbach J, Behrens C. Ultraviolet and soft X-ray free-electron lasers. In: *Introduction to Physical Principles, Experimental Results, Technological Challenges, STMP 229*. Berlin; Heidelberg: Springer (2008). doi: 10.1007/978-3-540-79572-8

30. Honkavaara K, Ackermann S, Ayvazyan V, Baboi N, Balandin V, Decking W, et al. *International Free-Electron Laser Conference (FEL2012, Nara)*. Report No. WEPD07. Status of the FLASH II Project (2012).

31. Ackermann S, Faatz B, Miltchev V, Rossbach J. *Proceedings of the 34th International Free-Electron Laser Conference* (FEL2012, Nara). Report No. TUPD11 (2012).

32. Schneidmiller E, Yurkov MV. *International Free-Electron Laser Conference* (FEL2013, New York, NY). Report No. WEPSO59.

33. Zagorodnov I, Dohlus M. Presentation at the Beam Dynamics meeting, DESY, Germany, (Accessed February 8, 2010). Available online at: http://www.desy.de/xfel-beam/data/talks/

34. Desy Flash. Available online at: http://www.desy.de/fel-beam/s2e/flash.html

35. Borland M. *ELEGANT: A Flexible SDDS-Compliant Code for Accelerator Simulation*. Argonne National Laboratory Advanced Photon Source Report No. LS-287 (2000).

36. Dohlus M, Limberg T. CSRtrack: Faster Calculation of 3D CSR effects. In: *26th International Free Electron Laser Conference*. Trieste (2004).

37. Hemsing E, Stupakov G, Xiang DA, Zholents A. Beam by design: laser manipulation of electrons in modern accelerators. *Rev Mod Phys.* (2014) **86**:897. doi: 10.1103/RevModPhys.86.897

38. Herrmann D, Veisz L, Tautz R, Tavella F, Schmid K, Pervak V, et al. Generation of sub-three-cycle, 16 TW light pulses by using noncollinear optical parametric chirped-pulse amplification. *Opt Lett.* (2009) **34**:2459–61. doi: 10.1364/OL.34.002459

39. Attosecond Light Pulse Source of the Extreme Light Infrastructure (ELI-ALPS). Available online at: http://www.eli-alps.hu/

40. Fattahi H, Barros HG, Gorjan M, Nubbemeyer T, Alsaif B, Teisset CY, et al. Third-generation femtosecond technology. *Optica* (2014) **1**:45–63. doi: 10.1364/OPTICA.1.000045

41. Hassan MT, Wirth A, Grguraš I, Moulet A, Luu TT, Gagnon J, et al. Invited Article: Attosecond photonics: synthesis and control of light transients. *Rev Sci Instrum.* (2012) **83**:11130. doi: 10.1063/1.4758310

42. Herrmann D, Homann C, Tautz R, Scharrer M, St. Russell JP, Krausz F, et al. Approaching the full octave: noncollinear optical parametric chirped pulse amplification with two-color pumping. *Opt Express* (2010) **18**:18752–62. doi: 10.1364/OE.18.018752

43. Jackson JD. *Classical Electrodynamics*. 3rd ed. New York, NY: Wiley (1999).

44. Ding Y, Huang Z, Ratner D, Bucksbaum P, Merdji H. Generation of attosecond x-ray pulses with a multicycle two-color enhanced self-amplified spontaneous emission scheme. *Phys Rev.* (2009) **12**:060703. doi: 10.1103/PhysRevSTAB.12.060703

45. Sansone G, Poletto L, Nisoli M. High-energy attosecond light sources. *Nat Photon.* (2011) **5**:655–63. doi: 10.1038/nphoton.2011.167

46. Zhao K, Zhang Q, Chini M, Wu Y, Wang X, Chang Z. Tailoring a 67 attosecond pulse through advantageous phase-mismatch. *Opt Lett.* (2012) **37**:3891. doi: 10.1364/OL.37.003891

47. Sansone G, Benedetti E, Calegari F, Vozzi C, Avaldi L, Flammini R, et al. Isolated single-cycle attosecond pulses. *Science* (2006) **314**:443–6. doi: 10.1126/science.1132838

48. Takahashi EJ, Lan P, Mücke OD, Nabekawa Y, Midorikawa K. Attosecond nonlinear optics using gigawatt-scale isolated attosecond pulses. *Nat Commun.* (2013) **4**:2691. doi: 10.1038/ncomms3691

49. Thaury C, Quéré F. High-order harmonic and attosecond pulse generation on plasma mirrors: basic mechanisms. *J Phys B At Mol Opt Phys.* (2010) **43**:213001. doi: 10.1088/0953-4075/43/21/213001